Applied Physics Letters ARTICLE scitation.org/journal/apl

Hybrid magnetoacoustic metamaterials for ultrasound control

Cite as: Appl. Phys. Lett. **117**, 102402 (2020); doi: 10.1063/5.0018801
Submitted: 18 June 2020 · Accepted: 27 August 2020 ·
Published Online: 10 September 2020

O. S. Latcham,[1] Y. I. Gusieva,[2] A. V. Shytov,[1] O. Y. Gorobets,[2] and V. V. Kruglyak[1,a)]

AFFILIATIONS

[1]University of Exeter, Stocker Road, Exeter EX4 4QL, United Kingdom
[2]Igor Sikorsky Kyiv Polytechnic Institute, 37 Prosp. Peremohy, Kyiv 03056, Ukraine

[a)]Author to whom correspondence should be addressed: V.V.Kruglyak@exeter.ac.uk

ABSTRACT

We propose a class of metamaterials in which the propagation of acoustic waves is controlled magnetically through magnetoelastic coupling. The metamaterials are formed by a periodic array of thin magnetic layers ("resonators") embedded in a nonmagnetic matrix. Acoustic waves carrying energy through the structure hybridize with the magnetic modes of the resonators ("Fano resonance"). This leads to a rich set of effects, enhanced by Bragg scattering and being most pronounced when the magnetic resonance frequency is close to or lies within acoustic bandgaps. The acoustic reflection from the structure exhibits magnetically induced transparency and Borrmann effect. Our analysis shows that the combined effect of the Bragg scattering and Fano resonance may overcome the magnetic damping, ubiquitous in realistic systems. This paves a route toward the application of such structures in wave computing and signal processing.

The minimization of energy loss in modern computing devices calls for unorthodox approaches to signal processing.[1,2] For instance, proposals to employ spin waves[3] as a data carrier to save energy in nonvolatile memory devices have promoted growth in the research area of magnonics.[4] However, these hopes are hampered by the short propagation distance of spin waves, caused by the magnetic damping.[5,6] Magnetostrictive materials offer a route to circumvent this. Indeed, acoustic waves have longer attenuation lengths as compared to spin waves at the same frequencies. In magnetostrictive materials, acoustic waves can still couple to spin waves, forming hybrid magnetoacoustic waves.[7–13] Thus, one regains the option of magnetic control and programmability, catering to the design of systems that evoke benefits of both acoustics and magnonics in terms of the energy efficiency.

The recently studied magnetoacoustic devices[11] and metamaterials[13] were typically formed using alternating magnetostrictive materials, so that the full acoustic and magnonic spectra were hybridized. To reduce the influence of the magnetic damping, we explored systems in which the magnetic loss was restricted to an isolated, thin-film magnetostrictive inclusion ("resonator"), hosting a single spin-wave mode, that of the ferromagnetic resonance (FMR).[14] The FMR mode hybridized with acoustic waves only near the Kittel frequency,[3] which led to their resonant scattering in a magnetoacoustic version of the Fano resonance.[15] The FMR mode's frequency and linewidth (and therefore the strength of the Fano resonance) were determined by the bias magnetic field and by the magnetic damping, respectively. Our analysis highlighted the need to enhance the (generally, weak) magnetoelastic interaction and to suppress the (generally, strong) magnetic damping, which was partly achieved by adopting an oblique incidence geometry. A question arises as to whether the effects of the magnetoelastic coupling could be enhanced even further due to Bragg scattering in magnetoacoustic metamaterials[13] formed by periodic arrays of the magnetoacoustic resonators introduced in Ref. 14.

In this Letter, we demonstrate that, by combining individual magnetoacoustic resonators into one-dimensional (1D) arrays (similar to locally resonant phononic crystals),[16] one can indeed significantly enhance their effect on incident acoustic waves. The acoustic reflectivity of such a metamaterial exhibits a peak due to the magnetoacoustic Fano resonance. The peak's height and shape can be tuned at frequencies in the proximity of phononic bandgaps. In particular, its behavior near the two edges of a bandgap exhibits a strong asymmetry, which is linked to the Borrmann effect.[17] Inside the bandgaps, we identify behavior reminiscent of the magnetically induced transparency.[15] These features of our prototypical metamaterial could be employed to process acoustic signals and engineer reconfigurable magnetoacoustic devices.

The building blocks of our metamaterials are thin ferromagnetic slabs (resonators) of thickness δ, infinite in the Y–Z plane, separated by nonmagnetic spacer layers of thickness δ_s ($\delta_s \gg \delta$), as shown in

Fig. 1(a). The slabs are magnetized by a bias magnetic field $\mathbf{H}_B = H_B\hat{\mathbf{z}}$ and have saturation magnetization M_s. The elastic properties of the magnetic and spacer materials may differ. The shear stress produced by propagating transverse acoustic waves perturbs the magnetization, as described by the standard magnetoelasticity theory.[7,9,18–20] The hybridization between the acoustic waves and the magnetization precession manifests itself as a Fano-like peak in the frequency dependence of the acoustic reflectivity [Fig. 1(b)].[14] This peak occurs near the Kittel frequency of the slab, f_{FMR}, and is therefore controlled by the bias magnetic field. The strength of the coupling between the propagating acoustic and localized magnetic modes is noticeably enhanced for an oblique incidence [Fig. 1(b)]. However, for realistic values of the magnetoelastic coupling, B, a noticeable effect requires rather small values of the Gilbert damping, e.g., $\alpha \simeq 10^{-3}$.

We aim to increase the interaction time of the acoustic waves with the magnetic slabs by slowing the waves down in the vicinity of phononic bandgaps. Hence, an enhancement of the magnetoacoustic response of such a structure can be expected when this anticrossing is tuned to the proximity of the phononic bandgap. So, we arrange the slabs into arrays, either containing N magnetic elements or semi-infinite. Let the nth resonator be situated at $x_n = nL$, where $L = \delta + \delta_s$ is the period of the array. Acoustic waves are obliquely incident on the array from the left. The magnetoacoustic response of finite arrays is characterized by the reflection, R_N, transmission, T_N, and absorption, A_N, coefficients. Using the transfer matrix method,[21] these coefficients can be expressed via the reflection, r, and transmission, t, coefficients in the forward direction together with the respective coefficients $\tilde{r}$, and $\tilde{t}$, in the backward direction. For normal incidence, reciprocity between forward and backward reflection is maintained ($r = \tilde{r}$). However, at oblique incidence, r and $\tilde{r}$ acquire different phases. The transmission and reflection coefficients for an individual slab are derived by considering the modes inside the slab and matching interfacial displacements and stresses with those of the incoming and outgoing elastic waves. The magnetoelastic interaction inside the slab can be included in the matching procedure adding relevant contributions to the stress[14,22,23] or the acoustic impedance.[14] For a thin slab, one can neglect exchange contribution to the effective magnetic field and treat magnetodipole interaction by introducing relevant demagnetizing coefficients.[14] As illustrated in Fig. 1(b), the resulting coefficients t, $\tilde{t}$, r, and $\tilde{r}$ exhibit a strong frequency dependence, indicative of the resonant hybridization between the acoustic and magnetic modes. The spectral function (derived in the supplementary material) of a phononic crystal with embedded magnetic slabs, as shown in Fig. 1(c), exhibits a magnetically tunable anticrossing with the usual phononic bandgap dispersion.

The transverse acoustic displacement $\boldsymbol{U} = U(x, y, t)\hat{\mathbf{z}}$ due to an obliquely incident acoustic wave inside the nth nonmagnetic spacer layer, $(n-1)L < x < nL - \delta$, is given by

$$U(x, y, t) = e^{-i\omega t + iq_y y}\left[A_n e^{i\phi_x} + B_n e^{-i\phi_x}\right], \tag{1}$$

where q represents the wave number in the nonmagnetic layer and $\phi_x = q_x[x - (n-1)L]$. In what follows, we retain only the x-dependence of the wave function. The amplitudes A_n and B_n are acoustic, traveling to the right and to the left in the nth nonmagnetic layer, respectively. Then, for a wave of unit amplitude incident from the left onto a finite array, we have $A_0 = 1$, $B_0 = R_N$, $A_N = T_N$, $B_N = 0$. To form the transfer matrix M for a single period of the array, amplitudes

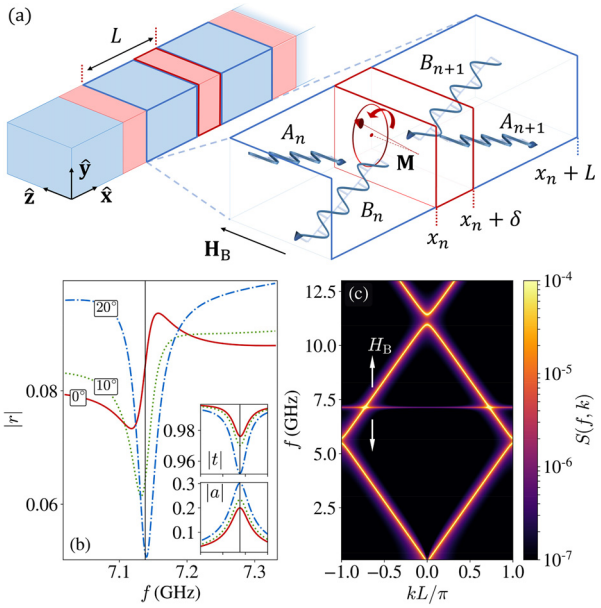

FIG. 1. (a) The problem geometry is schematically shown. The metamaterial is formed by a 1D array of thin-film magnetoacoustic resonators embedded in a nonmagnetic matrix. Individual resonators scatter acoustic waves incident from both sides. A bias magnetic field $\mathbf{H}_B$ is applied in the resonator's plane. (b) The frequency dependence of the reflection coefficient, r, for incidence angles ranging from 0° to 20° is shown for an isolated Co resonator in a silicon nitride matrix. The vertical line indicates the Kittel frequency for a field of $\mu_0 H_B = 50$ mT and $\alpha = 10^{-3}$. The inset shows the corresponding transmission, t, and absorption, a, coefficients. (c) The spectral function, $S(f, k)$, of acoustic waves in the metamaterial is shown. The frequency of the anticrossing is controlled by the bias magnetic field, which has a value of $\mu_0 H_B = 50$ mT here.

at $x = nL$ and $x = (n+1)L$ can be related via forward (t, r) and backward ($\tilde{t}$, $\tilde{r}$) transmission and reflection coefficients. Waves in neighboring segments can be matched by treating them as "black boxes" with the given transmission and reflection coefficients. Hence, we write for the interface between the nth and $(n+1)$th segment:

$$\begin{aligned} A_{n+1}\exp(-i\chi_\theta) &= tA_n + \tilde{r}B_{n+1}\exp(i\chi_\theta), \\ B_n &= \tilde{t}B_{n+1}\exp(i\chi_\theta) + rA_n, \end{aligned} \tag{2}$$

where $\chi_\theta = \omega\delta_s\cos\theta\sqrt{\rho/C}$ is the acoustic phase delay within the spacer layer. The transfer matrix M links the vector (A_{n+1}, B_{n+1}) to (A_n, B_n) and is constructed by inverting Eq. (2) as

$$M = \begin{Bmatrix} [t - \tilde{r}r\tilde{t}^{-1}]\exp(i\chi_\theta) & \tilde{r}\tilde{t}^{-1}\exp(i\chi_\theta) \\ -r\tilde{t}^{-1}\exp(-i\chi_\theta) & \tilde{t}^{-1}\exp(-i\chi_\theta) \end{Bmatrix}. \tag{3}$$

The action of M can be represented by its eigenvalues $\mu_\pm$ and the respective eigenvectors. The eigenvalues that solve the characteristic equation $\mu^2 - 2\mathscr{T}\mu + d = 0$ are given by $\mu_\pm = \mathscr{T} \mp \sqrt{\mathscr{T}^2 - \mathscr{D}}$, where $\mathscr{D} \equiv \det M = \mu_+\mu_-$ and $2\mathscr{T} \equiv \mathrm{Tr}M = \mu_+ + \mu_-$. From Eq. (3), we find that $\mathscr{D} = t/\tilde{t}$, which has an absolute value of one. As usual, we find that the two eigenvalues of M either both lie on the unit circle $|\mu| = 1$ or one is inside and the other is outside. In our system,

the energy is dissipated due to the Gilbert damping. Hence, we can define $\mu_\pm$ so that $|\mu_+| < 1$, representing the wave propagating to the right. For a finite array of N resonators, the full transfer matrix $M_N = M^N$ retains the eigenvector basis with eigenvalues $\mu_\pm^N$. The initial and final state amplitudes are then projected onto a reciprocal of this basis, multiplied by the eigenvalues, and resolved to obtain for the finite array's reflection coefficient,

$$R_N = \frac{R_\infty\left(1-\mu^{2N}\right)}{\left(1-\xi\mu^{2N}\right)}, \tag{4}$$

where R_∞ is the reflection from a semi-infinite array,

$$R_\infty = r\exp\left(-i\chi_\theta\right)\left[\tilde{t}\mu_- - \left(t\tilde{t}-r\tilde{r}\right)\exp(i\chi_\theta)\right]^{-1}, \tag{5}$$

and ξ is defined as

$$\xi = \frac{\left(t\tilde{t}-r\tilde{r}\right)\exp(i\chi_\theta)-\tilde{t}\mu_+}{\left(t\tilde{t}-r\tilde{r}\right)\exp(i\chi_\theta)-\tilde{t}\mu_-}. \tag{6}$$

The transmission coefficient of a finite length array has the form

$$T_N = \frac{(1-\xi)\mu_+^N}{1-\xi\mu^{2N}}. \tag{7}$$

Detailed derivation of Eqs. (4) and (7) is given in Sec. I of the supplementary material. The absorbance is found as $A_N^2 = 1-|R_N|^2-|T_N|^2$. In what follows, we omit the explicit dependence of the quantities ξ and μ upon the frequency, ω, and the phase delay, χ_θ.

To illustrate how R_N depends on the number of elements in a finite array, we have performed detailed calculations for an array of resonators with parameters equal to those from Ref. 24: mass density $\rho = 8900\,\mathrm{kg\,m^{-3}}$, magnetoelastic coupling coefficient $B = 8.8\,\mathrm{MJ\,m^{-3}}$, shear modulus $C = 76\,\mathrm{GPa}$, gyromagnetic ratio $\gamma = 31.7\,\mathrm{GHz\,T^{-1}}$, and saturation magnetization $M_s = 203\,\mathrm{kA\,m^{-1}}$, $\delta = 30\,\mathrm{nm}$. The matrix is silicon nitride [$\rho_0 = 3192\,\mathrm{kg\,m^{-3}}$, $C_0 = 127\,\mathrm{GPa}$, $\delta_s = 500\,\mathrm{nm}$ (Refs. 25 and 26)]. Figure 2 presents the results of the calculations for a generic case, without fine-tuning of the magnetoelastic resonance. For $N > 1$, the absolute value of the reflection coefficient reaches unity in frequency regions corresponding to the acoustic stopbands (phononic bandgaps). These are caused by the mismatch of the acoustic impedance $Z = \sqrt{\rho C}$ at the surface of the slabs, which occur even in the absence of the magnetoelastic coupling ($B = 0$).[27–29] Each passband contains $N-1$ peaks, which are due to the phase delay of the acoustic waves increasing by π across each Brillouin zone.[21] The magnetoelastic coupling ($B \neq 0$) manifests itself via an asymmetric peak due to the Fano resonance, positioned at the Kittel frequency $f_{\mathrm{FMR}} = \gamma\mu_0\sqrt{H_B(H_B+M_s)} \simeq 8.8\,\mathrm{GHz}$ at $\mu_0 H_B = 180\,\mathrm{mT}$.[7] The frequency dependences of T_N and A_N are given in the supplementary material for a complete picture.

The rapid oscillation in passbands in Fig. 2 is formed due to the multiple reflections within arrays of finite size. For sufficiently large arrays (i.e., when the decay length is smaller than the array size), these oscillations are suppressed. Indeed, the oscillations are suppressed for R_∞ [calculated using Eq. (5) and shown by the solid line in Fig. 2], as expected for $N \to \infty$. So, our subsequent analysis is focused on the semi-infinite array.

Figure 3 displays the reflectivity R_∞, of a semi-infinite array as a function of the frequency for different values of the bias magnetic field.

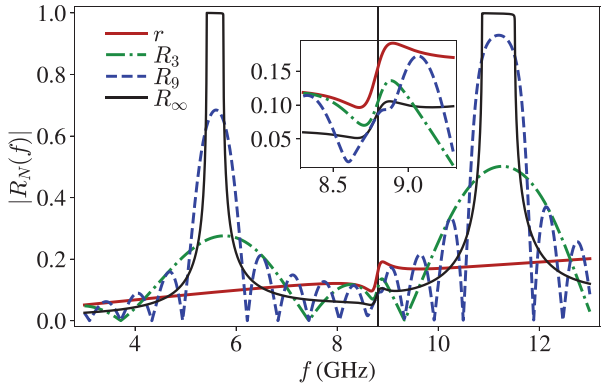

FIG. 2. The frequency dependence of the reflection coefficient, R_N, calculated using Eq. (4) for $N = 1$ (i.e., r), $N = 3$, and $N = 9$, is compared to that for a semi-infinite array, R_∞, calculated using Eq. (5). We assume $\alpha = 10^{-2}$ and $\mu_0 H_B = 180$ mT. The solid vertical line indicates the Kittel frequency, f_{FMR}, and the inset is focused around the region of the magnetoacoustic Fano resonance.

We identify two regimes based on the position of the Kittel frequency, f_{FMR}, relative to phononic bandgaps. Regime I occurs when f_{FMR} is tuned inside a passband, away from band edges. This is shown in Fig. 3(a), with insets comparing R_∞ and r. The peak in R_∞ is lower than that in r both when f_{FMR} is located in the passbands above and below the stop band, away from band edges. This suppression is caused by the destructive interference of waves reflected backward from different resonators.

Regime II occurs when the Kittel frequency, f_{FMR}, either falls within the bandgap [Fig. 3(b)] or approaches it from a passband [Fig. 3(c)]. Here, the resonant scattering becomes highly sensitive to the detuning of f_{FMR} from the band edge, differently affecting the scattering of acoustic waves with frequencies within the bandgap and adjacent passbands. In the passbands in close proximity to the bandgap, where the Bragg condition holds, the scattering is enhanced by the constructive interference of waves reflected backward from different resonators. In the bandgaps, the reflectivity is reduced from unity, as seen best in Fig. 3(b). This may be interpreted as a magnetically induced transparency, which is further supported by our analysis of the acoustic scattering from finite arrays, which is described in the supplementary material.

This reduction of reflectivity is not symmetric as the bias field sweeps the Kittel resonance frequency across the bandgap. The behavior at the upper and the lower bandgap edges is distinctly different: the reduction of reflectivity is stronger as f_{FMR} approaches the upper bandgap edge. This can be attributed to the Borrmann effect.[30,31] In a pure phononic crystal ($B = 0$), the modes at the band edges are two standing waves, phase shifted by 90°.[32] For one of the modes, the maxima of the stress occurs within the magnetic slabs, while for the other, this pattern is reversed: the slabs become the nodes. With the Gilbert damping being the primary mechanism of energy dissipation, absorption is suppressed for the mode that has nodes at the magnetic slabs, similar to Refs. 17 and 33. This condition is realized at the lower bandgap edge if the acoustic impedance of the magnetic (M) material is greater than that of the nonmagnetic matrix (NM), i.e., $Z_{\mathrm{M}} > Z_{\mathrm{NM}}$ (Fig. 3). The situation is reversed when $Z_{\mathrm{M}} < Z_{\mathrm{NM}}$. At the influenced

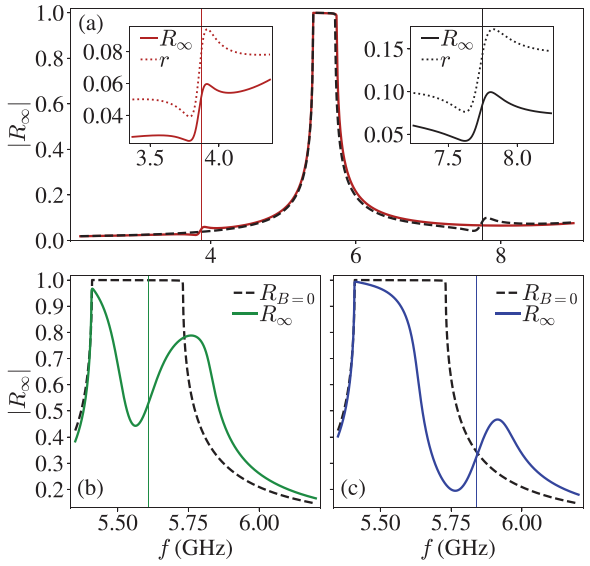

FIG. 3. The frequency dependence of the acoustic reflection coefficient, R_∞, from a semi-infinite array with $\alpha = 10^{-2}$ is shown for three different values of the Kittel frequency, f_{FMR}, tuned by the bias magnetic field, H_B. The solid vertical lines indicate the position of f_{FMR}. The dashed black curve represents $R_{B=0}$, i.e., R_∞ for $B = 0$. (a) Regime I: f_{FMR} is in the passband, far from the phononic bandgap. The insets compare R_∞ (solid) with r (dotted) at $\mu_0 H_B = 50$ mT (left, red) and 150 mT (right, black). Regime II: (b) f_{FMR} at $\mu_0 H_B = 92$ mT is inside the bandgap, and (c) f_{FMR} at $\mu_0 H_B = 98$ mT is close to the bandgap.

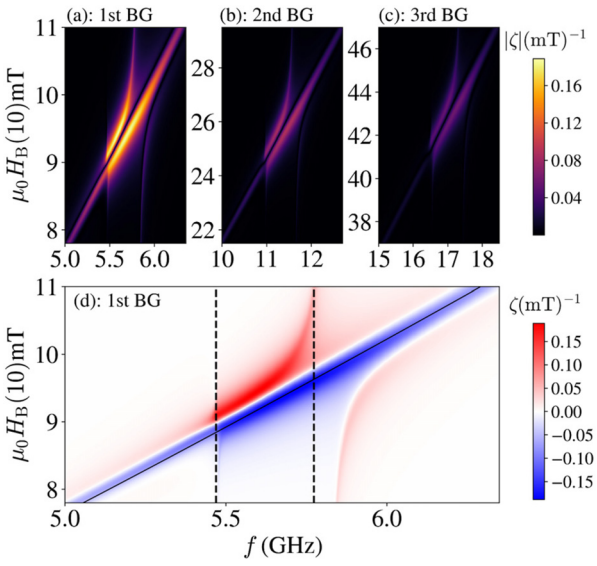

FIG. 4. The frequency and field dependence of the absolute value of the modulation coefficient, $|\zeta| = |\partial|R_\infty|/\partial H_B|$, is shown around the (a) first, (b) second, and (c) third phononic bandgaps. The solid white lines represent f_{ME}. (d) The frequency and field dependence of the modulation coefficient, $\zeta = \partial|R_\infty|/\partial H_B$, is shown around the first phononic bandgap. The position of the bandgap edges at $B = 0$ is marked with dashed vertical lines, and the solid black line represents f_{ME}. In all panels, $\alpha = 10^{-2}$.

edge, a shift in the edge frequency is induced by proximity to the Kittel frequency f_{FMR}.[34] This band shift is separate from the induced transparency; this becomes apparent when f_{FMR} sweeps a bandgap with a width significantly exceeding the Fano resonance linewidth, as shown in the supplementary material. We emphasize that the magnetoelastic effects shown in Fig. 3 remain significant even for a realistic damping value of $\alpha = 10^{-2}$. This is a considerable improvement compared to a single resonator where this damping value would completely suppress the Fano resonance.[14]

To characterize the tunability of the acoustic reflection coefficient by the bias magnetic field, we introduce the field modulation coefficient $\zeta = \partial|R_\infty|/\partial H_B$, the frequency and field dependence of which around the first three phononic bandgaps is shown in Fig. 4. In practice, the higher frequency phononic bandgaps could be more difficult to access, as this would require a large bias magnetic field (>0.25 T). Hence, we limit our analysis to frequencies around the first bandgap [Fig. 4(d)]. We see that ζ is significantly enhanced when f_{FMR} (solid, black) is tuned to the proximity of the bandgap edges (vertical, dashed, black), as expected for a Fano resonance induced modulation of scattering coefficients.[15] The strength of the Fano resonance is determined by the interplay between the damping and the strength of the magnetoelastic coupling.[14] The damping in our metamaterial is modulated by the Borrmann effect. This leads to an asymmetry of the field modulation coefficient with regard to the lower and higher frequency edges of the phononic bandgap [Fig. 4(d)].

In summary, we have shown that the metamaterial approach is indeed helpful for magnetoacoustics. Our hybrid metamaterials, formed by 1D arrays of resonators, magnify the effect of magnetoelastic coupling upon the acoustic scattering, thereby mitigating the Gilbert damping to tolerable levels. The scattering is tunable by a bias magnetic field and exhibits a rich and complex behavior, such as the induced transparency and Borrmann effect. The next step toward realistic structures and devices would be to extend the model into the second and third dimensions and to consider surface acoustic waves. However, the design strategies presented here will remain useful. Our results may help in engineering magnetoacoustic sensors, actuators, radio frequency modulators, and other devices that could benefit from the enhanced magnetic field modulation of the amplitude or the phase of acoustic waves, as demonstrated here.

See the supplementary material for (i) the derivation of the reflection and transmission coefficients for finite arrays of scatterers, (ii) the derivation of the phonon spectral function, (iii) additional figures for the transmission and absorbance for finite arrays, and (iv) signatures of magnetically induced transparency.

The research leading to these results has received funding from the Engineering and Physical Sciences Research Council of the United Kingdom (Grant Nos. EP/T016574/1 and EP/L015331/1) and from the European Union's Horizon 2020 research and innovation program under Marie Sklodowska-Curie Grant Agreement No. 644348 (MagIC).

DATA AVAILABILITY

The data that support the findings of this study are available within the article and its supplementary material.

REFERENCES

[1]G. P. Perrucci, F. H. P. Fitzek, and J. Widmer, "Survey on energy consumption entities on the smartphone platform," in IEEE Vehicular Technology Conference (2011), Vol. 73, p. 1.

[2]S. Manipatruni, D. E. Nikonov, and I. A. Young, "Beyond CMOS computing with spin and polarization," Nat. Phys **14**, 338 (2018).

[3]A. G. Gurevich and G. A. Melkov, *Magnetization Oscillations and Waves* (Chemical Rubber Corporation, New York, 1996).

[4]V. V. Kruglyak, S. O. Demokritov, and D. Grundler, "Magnonics," J. Phys. D **43**, 264001 (2010).

[5]V. N. Krivoruchko, "Spin waves damping in nanometre-scale magnetic materials (review article)," Low Temp. Phys. **41**, 670 (2015).

[6]S. Azzawi, A. T. Hindmarch, and D. Atkinson, "Magnetic damping phenomena in ferromagnetic thin-films and multilayers," J. Phys. D **50**, 473001 (2017).

[7]C. Kittel, "Interaction of spin waves and ultrasonic waves in ferromagnetic crystals," Phys. Rev. **110**, 836 (1958).

[8]H. Bömmel and K. Dransfeld, "Excitation of hypersonic waves by ferromagnetic resonance," Phys. Rev. Lett. **3**, 83 (1959).

[9]E. Callen and H. B. Callen, "Magnetostriction, forced magnetostriction, and anomalous thermal expansion in ferromagnets," Phys. Rev. **139**, A455 (1965).

[10]L. Dreher, M. Weiler, M. Pernpeintner, H. Huebl, R. Gross, M. Brandt, and S. Goennenwein, "Surface acoustic wave driven ferromagnetic resonance in nickel thin films: Theory and experiment," Phys. Rev. B **86**, 134415 (2012).

[11]A. Kamra, H. Keshtgar, P. Yan, and G. E. W. Bauer, "Coherent elastic excitation of spin waves," Phys. Rev. B **91**, 104409 (2015).

[12]T. Kikkawa, K. Shen, B. Flebus, R. A. Duine, K. Uchida, Z. Qiu, G. E. W. Bauer, and E. Saitoh, "Magnon polarons in the spin Seebeck effect," Phys. Rev. Lett. **117**, 207203 (2016).

[13]P. Graczyk, J. Kłos, and M. Krawczyk, "Broadband magnetoelastic coupling in magnonic-phononic crystals for high-frequency nanoscale spin-wave generation," Phys. Rev. B **95**, 104425 (2017).

[14]O. S. Latcham, Y. I. Gusieva, A. V. Shytov, O. Y. Gorobets, and V. V. Kruglyak, "Controlling acoustic waves using magneto-elastic Fano resonances," Appl. Phys. Lett. **115**, 082403 (2019); see also **116**, 209902 (2020) for an erratum and arXiv:1911.06774 for an updated version of the paper.

[15]M. F. Limonov, M. V. Rybin, A. N. Poddubny, and Y. S. Kivshar, "Fano resonances in photonics," Nat. Photonics **11**, 543 (2017).

[16]Y. Xio, B. R. Mace, J. Wen, and X. Wen, "Formation and coupling of band gaps in a locally resonant elastic system comprising a string with attached resonators," Phys. Lett. A **375**, 1485 (2011).

[17]V. B. Novikov and T. V. Murzina, "Borrmann effect in photonic crystals," Opt. Lett. **42**, 1389 (2017).

[18]R. L. Comstock and B. A. Auld, "Parametric coupling of the magnetization and strain in a ferrimagnet. I. Parametric excitation of magnetostatic and elastic modes," J. Appl. Phys. **34**, 1461 (1963).

[19]A. I. Akhiezer, V. G. Bar'yakhtar, and S. V. Peletminskii, *Spin Waves* (North-Holland, Amsterdam, 1968).

[20]E. Schlömamm, "Generation of phonons in high-power ferromagnetic resonance experiments," J. Appl. Phys. **31**, 1647 (1960).

[21]P. Markos and C. M. Sokoulis, *Wave Propagation* (Princeton University Press, 2008).

[22]H. S. Streib and G. E. W. Bauer, "Damping of magnetization dynamics by phonon pumping," Phys. Rev. Lett. **121**, 027202 (2018).

[23]A. Rückriegel and R. A. Duine, "Long-range phonon spin transport in ferromagnet-nonmagnetic insulator heterostructures," Phys. Rev. Lett. **124**, 117201 (2020).

[24]C. Berk, M. Jaris, W. Yang, S. Dhuey, S. Cabrini, and H. Schmidt, "Strongly coupled magnon-phonon dynamics in a single nanomagnet," Nat. Commun. **10**, 2652 (2019).

[25]R. Huszank, L. Csedreki, Z. Kertész, and Z. Török, "Determination of the density of silicon-nitride thin films by ion-beam analytical techniques (RBS, PIXE, STIM)," J. Radioanal. Nucl. Chem. **307**, 341 (2016).

[26]A. C. Inc., see http://www.matweb.com/index.aspx for "MatWeb: Material Property Data 2019" (last accessed November 14, 2019).

[27]P. Martin, I. Abrahams, and W. Parnell, "One-dimensional reflection by a semi-infinite periodic row of scatterers," Wave Motion **58**, 1 (2015).

[28]M. Born and E. Wolf, *Principles of Optics* (Pergamon, Oxford, New York, 1964).

[29]L. M. Brekhovskikh and O. A. Godin, *Acoustics of Layered Media* (Springer, Berlin/Heidelberg, 1997).

[30]H. N. Campbell, "X-ray absorption in a crystal set at the Bragg angle," J. Appl. Phys. **22**, 1139 (1951).

[31]B. W. Batterman and H. Cole, "Dynamical diffraction of x-rays by perfect crystals," Rev. Mod. Phys. **36**, 681 (1964).

[32]C. Croënne, E. J. S. Lee, H. Hu, and J. H. Page, "Band gaps in phononic crystals: Generation mechanisms and interaction effects," AIP Adv. **1**, 041401 (2011).

[33]V. V. Kruglyak and A. N. Kuchko, "Effect of the modulation of magnetic viscosity on the damping of spin waves in multilayer magnetic systems," Phys. Met. Metallogr. **92**, 3 (2001).

[34]T. Kobayashi, R. C. Barker, J. L. Bleustein, and A. Yelon, "Ferromagnetoelastic resonance in thin films. I. Formal treatment," Phys. Rev. B **7**, 3273 (1973).